Extended x-ray-absorption fine-structure study of alkali-metal halides under high pressure

J. Freund* and R. Ingalls
Department of Physics, University of Washington, Seattle, Washington 98195

E. D. Crozier
Department of Physics, Simon Fraser University, Burnaby, British Columbia, Canada V5A 1S6
(Received 9 November 1990; revised manuscript received 18 March 1991)

The extended x-ray-absorption fine structure (EXAFS) of three alkali-metal halides (NaBr, KBr, and RbCl) is investigated at pressures ranging from 0 to 8 GPa. Parameter fitting is used to extract the change of the nearest-neighbor distance and thus the pressure, as well as the absolute values of the second cumulant as a function of pressure, $\sigma^2(p)$, and the third cumulant at zero pressure, $\sigma^{(3)}(0)$. For all three materials, a sharp reduction with pressure of $\sigma^2(p)$ is found. Classical statistical mechanics is then invoked to calculate the first, second, and third moments of the nearest-neighbor distance and thus their second and third cumulants. The integration is done with the Monte Carlo technique. For the potential energy U in the Boltzmann factor, the generalized Huggins-Mayer pair potential is used along with a three-body potential term due to charge transfer. Generally, model calculations and EXAFS data match well. High-pressure EXAFS data can therefore be regarded as a help to assess, and even exclude, potential parameters from the literature.

I. INTRODUCTION

The study of the extended x-ray-absorption fine structure (EXAFS) of materials under high pressure has been limited to a few research groups worldwide. It differs from zero-pressure EXAFS studies insofar as a large fraction of the incident radiation is absorbed by the anvils that exert pressure on the sample. This has two consequences: (i) low-Z elements cannot be studied; (ii) very high fluxes are required for the other elements. This excludes laboratory x-ray sources, leaving only synchrotron-radiation sources. Since the loss of photons is so great and the samples are so small, the signal-to-noise ratio is less favorable than with zero-pressure experiments.

Notwithstanding these adverse limiting conditions, successful high-pressure measurements of the x-ray-absorption near-edge structure (XANES) and the EXAFS (together referred to as x-ray-absorption fine structure, or XAFS) have been reported in recent years. A list of high-pressure EXAFS papers since 1986 is given in the reference section.[1–22] The studies concentrated on pressure-volume relations and on the structural changes accompanying pressure-induced first- and second-order phase transitions. Quantitative analysis of the EXAFS was concerned mostly with determining the nearest-neighbor distance, coordination number, and second cumulant σ^2 [or EXAFS Debye-Waller factor, $\exp(-2k^2\sigma^2)$]. Multiple-scattering contributions to the structural specification of the next-nearest neighbor have also been considered.[12]

Recently efforts[7,20] have been made to understand the pressure dependence of the second cumulant of the nearest-neighbor distance. The second cumulant is related to the first and second moments as given by Eq. (2a) below. It has been conjectured[7] that three-body exchange interactions have to be introduced to obtain a full understanding of the second cumulant of solid krypton.

In this paper we extend the connection between cumulants and interatomic potentials. We have already shown in a previous paper[21] that the introduction of three-body interactions is helpful to understand the deviation of the amorphous germanium bond compressibility from that of crystalline germanium. We will show here that Monte Carlo calculations of the second and third cumulants of three alkali-metal halides (NaBr, KBr, and RbCl) depend on the parametrization of the pair potential and that the introduction of a three-body interaction makes a difference.

At the present time we still fall short of fitting potential parameters from high-pressure EXAFS data, but the strong dependence of the second cumulants on interatomic potentials suggests that this will be feasible in the future with the advent of higher-flux x-ray sources, thus rendering high-pressure EXAFS a new probe in solid-state physics.

The plan of this paper is as follows. In Sec. II we summarize the experiment and indicate data-analysis procedures. For brevity, definitions and equations pertaining to EXAFS and the cumulant expansion have not been repeated. The reader is referred to our previous paper on copper.[20] The experimental results are given in Sec. III. In Sec. IV the cumulants are calculated using the Monte Carlo technique. Different models used for the potential energy of the crystal are described. Finally in Sec. V, the extent to which the second cumulant is sensitive to the potential parameters is shown.

II. EXPERIMENTATION AND DATA ANALYSIS

The setup of our high-pressure XAFS experiment was described in previous papers.[20,23] The samples in the ex-

periments described here consisted of finely ground powders of NaBr, KBr, and RbCl mixed with epoxy. We had some samples with two alkali-metal halides (KBr+RbCl and NaBr+RbCl) and some samples with one halide and another substance (NaBr+X and RbCl+X). Since our interest in alkali-metal halides originated in the need to have a pressure calibrant, the former samples were used to check our ability to extract pressures correctly from the reduction of nearest-neighbor distances. The latter samples, on the other hand, did act as pressure calibrants for the study of the other materials X.

Absorption spectra were taken in transmission at the K edges of bromine (NaBr and KBr) and rubidium (RbCl). All experiments were performed at beamline 4-1 of the Stanford Synchrotron Radiation Laboratory (SSRL) over a period of 10 years. The data were taken with either Si(111) or Si(220) crystals. For the Si(111) crystal, there is negligible intensity beyond about 17 keV; so higher-harmonic contamination is not a problem. For the Si(220) crystal, the monochromator was always detuned, typically by 50%, by slightly misaligning the second crystal.

The extraction of a single-shell EXAFS spectrum is a nontrivial operation that requires considerable trial and error. We first checked whether the EXAFS amplitude is affected by a convolution with the spectrum of the nominally monochromatic radiation impinging on the sample in spite of our setting the entrance slit width to only 1 mm. We assumed a Gaussian spectrum of half-width W, and did successive deconvolutions with increasing W until spurious noise started to emerge in the deconvoluted data (at about $W=0.5$ eV). Since no change of the amplitude was noticeable up to that point, deconvolution is not a necessary step in our data analysis. The data were then deglitched and the high-energy tails truncated in order to facilitate the background removal. $k=0$ was always set at the maxima of the XANES.

The post-edge background removal requires careful attention since it determines the quality of the Fourier transform at low r which is essential for a good back-transform over as wide an r range as possible. We found the IMSL subroutine ICSSCU,[24] as described by Cook and Sayers,[25] the most suitable choice. The two free parameters—the weighting factor and the smoothing parameter—were chosen interactively and the backgrounds as well as their first derivatives were plotted on screen before a decision was made. After background subtraction, the data were divided by the step height in the usual fashion to obtain the $\chi(k)$ spectrum.

Data sets pertaining to one pressure were then averaged and the amplitudes were renormalized with the McMaster tables:[26] The McMaster coefficients of the pre-edge absorption were extrapolated, subtracted from the McMaster post-edge absorption, and normalized to unity at the absorption edge. The data were then divided by that function. It produced a 1–3 % decrease in σ^2 for the alkali-metal halides considered (and can be much higher in other materials and at the L edge).

Further data analysis went as follows.

NaBr: The $\chi(k)$ spectrum (Fig. 1) was weighted with $k^{2.5}$. The exponent x of the weighting is determined by the consideration that the amplitude of the $\chi(k)k^x$ spectrum should be symmetric in the k range used or, conversely, the amplitude should be minimal at the cutoff points. A Gaussian window with full height at 4.8 Å^{-1} and 10% heights at 1.3 and 8.3 Å^{-1} was then applied and the Fourier transform into **r** space was performed. The fact that NaBr remains in the $B1$, or NaCl, structure throughout the pressure range investigated makes the separation in **r** space of first and second shells easy. The backtransform into **k** space was performed after application of a boxcar window to the first shell, taking the full-width at 25% of the maximum as a guideline.

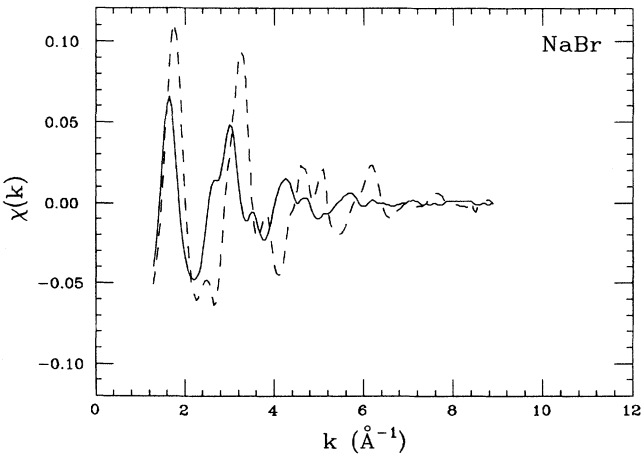

FIG. 1. EXAFS interference function $\chi(k)$ of NaBr at 0.0 GPa (solid curve) and 5.9 GPa (dashed curve).

KBr: The $\chi(k)$ spectrum (Fig. 2) of the $B1$ ($B2$) structure was weighted with k^2 (k^3) and the Gaussian window was again applied over the entire range of the spectrum with full height at 4.9 Å^{-1} (6.4 Å^{-1}) and 10% heights at 1.4 and 8.4 Å^{-1} (11.4 Å^{-1}). This data preparation technique produces a resolution in **r** space that allows separation of first and second shells even in the $B2$, or CsCl, structure which KBr assumes above 1.7 GPa. In the

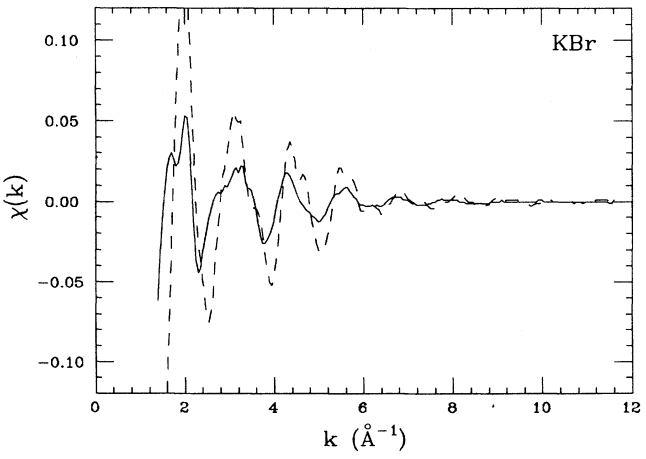

FIG. 2. EXAFS interference function $\chi(k)$ of KBr at 0.0 GPa (solid curve) and 6.1 GPa (dashed curve).

CsCl structure the ratio of second- to first-nearest-neighbor distances, R_2/R_1, is only 1.15, as opposed to 1.41 in the NaCl structure. At the highest pressure of this study, $R_2=3.65$ Å and $R_1=3.16$ Å.

RbCl: The data (Fig. 3) were weighted with k^3 and the Gaussian window was placed in a way analogous to those for NaBr and KBr, with a k range from 1.5 to 10.5 Å^{-1}. Again, the fact that RbCl undergoes the $B1$-$B2$ phase transition at 0.5 GPa had no influence on our ability to extract single-shell data. Without single-shell data several more parameters would have to be fitted, rendering the fit results less reliable.

The single-shell data thus produced were fitted to the single-scattering EXAFS formula including cumulants up to third order,

$$\chi(k)=A(k)\sin[\Psi(k)] , \tag{1a}$$

with the amplitude

$$A(k)=\frac{NF(k,\pi)f}{kR^2}e^{-2R/\lambda(k)}e^{-2\sigma^2k^2} \tag{1b}$$

and the phase

$$\Psi(k)=2k\left[R-\frac{2\sigma^2}{R}\left[1+\frac{R}{\lambda(k)}\right]\right]-\frac{4}{3}\sigma^{(3)}k^3+\Phi(k) . \tag{1c}$$

Here, N is the coordination number; $F(k,\pi)$, the backscatter amplitude; f, an as-yet-undetermined amplitude-correction factor; R, the distance to the shell; $\lambda(k)$, the electron mean free path; σ^2, the second cumulant; $\sigma^{(3)}$, the third cumulant; and $\Phi(k)$, the combined central-atom and backscatter phase shift. k is the electron wave vector. Since it depends on a convenient but nonetheless arbitrary choice of zero, it must be related to the real wave vector k' (in units of Å^{-1}) by

$$k=\left[(k'^2)-\frac{\Delta E}{3.81}\right]^{1/2} , \tag{1d}$$

where ΔE (in units of eV) is the shift between the assumed and the real zero of the free-electron states.

While N is known, $F(k,\pi)$, $\lambda(k)$, and $\Phi(k)$ were taken from the F_{eff} calculations (version 3.23) of Rehr, Albers, and Mustre de Leon.[27] This leaves f, R, σ^2, $\sigma^{(3)}$, and ΔE as fit parameters. We fitted the data in two steps.

(i) f, R, σ^2, and ΔE were fitted, with $\sigma^{(3)}$ set equal to zero. f and ΔE were then averaged over all NaBr data sets and separately over all $B1$- and $B2$-structure data sets of KBr and RbCl. The fitting was done by producing a model $\chi(k)$, subjecting it to the same Fourier forward transform and backtransform as the experimental $\chi(k)$, and then successively changing the parameters until the model $\chi(k)$ and the experimental $\chi(k)$ converge. f was found to be 0.64, 0.48, and 0.70 for NaBr, KBr, and RbCl, respectively.

(ii) R, σ^2, and $\sigma^{(3)}$ were fitted, with f and ΔE taken as constants. We found that different values for ΔE have to be used when a structural phase transition is observed (KBr and RbCl) because the XANES changes, and with it the reference point that we pick to denote the zero of the free-electron states ($k=0$).

Once the changes in the nearest-neighbor distances have been extracted, the Murnaghan isothermal equation of state[28] is used along with the compression values of Vaidya and Kennedy[29] to determine the pressure. More recent references[30,31] confirm the $B1$-$B2$ transition pressures quoted by them.

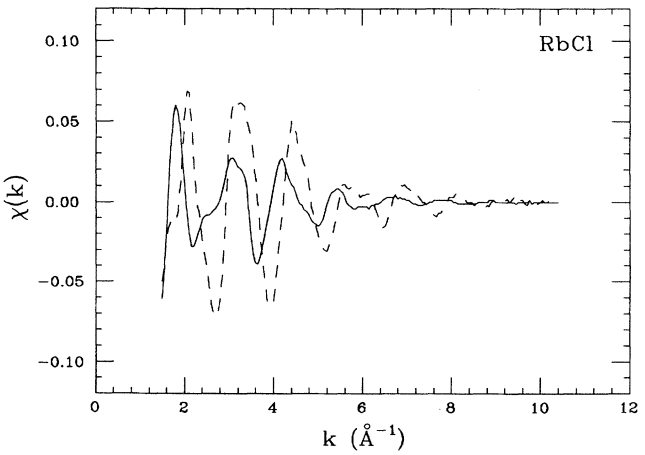

FIG. 3. EXAFS interference function $\chi(k)$ of RbCl at 0.0 GPa (solid curve) and 7.7 GPa (dashed curve).

III. EXPERIMENTAL RESULTS

Generally, we have not put much emphasis on observing the $B1$-$B2$ phase transition since it is rather difficult to apply exactly the right pressure. In most cases the Fourier transforms jump from the $B1$ phase into the $B2$ phase as shown in Fig. 4(a), with the position of the first shell remaining almost stationary but the second-shell position of RbCl changing from 4.66 Å at 0 GPa to 3.91 Å at 0.5 GPa. As usual, the peaks in the Fourier transforms are shifted to smaller distances due to the central-atom and backscatter phase shifts in the EXAFS phase. Only in one instance did we actually observe the phase transition of RbCl [Fig. 4(b)], i.e., Fourier transforms that are intermediate between the $B1$ and $B2$ phases.

In Fig. 5 pressures determined from samples containing KBr and RbCl (cross symbol) or NaBr and RbCl (diamond symbol) are plotted. Ideally, all symbols should be aligned along the diagonal, shown by a solid line. At first we tried to set $\sigma^{(3)}$ equal to zero in the second round of parameter fitting, as described above. The result, depicted in Fig. 5(a), indicates considerable random errors. When $\sigma^{(3)}$ is taken into account [Fig. 5(b)], the random scatter of the points is sharply reduced. However, a slight systematic deviation from the diagonal remains: The upper (lower) dotted line represents the straight-line fit of the KBr+RbCl (NaBr+RbCl) symbols. It seems that the pressures determined from RbCl are slightly

higher than those determined from KBr and NaBr, especially at higher pressures. We determined the average distance of the symbols from the diagonal to be 0.3 GPa and assigned this value to the error bars in the diagrams to follow.

Figures 6–8 show second cumulants σ^2 of the nearest-neighbor distances. Single experimental results are represented by diamonds, weighted-least-squares fits of the experimental results are shown by continuous lines of cross symbols. The inverse of the goodness-of-fit parameter was used as a weight. The standard deviations of all zero-pressure data sets (7 for NaBr, 3 for KBr, and 11 for RbCl) were calculated and serve as error bars. Standard deviations for nonzero pressures could not be calculated, since most of the nonzero pressures occurred only once. Nonstatistical errors due to different types of data preparation (background removal, Fourier forward transform and backtransform) are about $(0.1-0.2)\times10^{-3}$ Å^2, i.e., negligible. Note that further systematic errors cannot be excluded due to the correlation of σ^2 with the F_{eff} values for $F(k,\pi)e^{-2R/\lambda(k)}$ and due to the fact that f is an unknown quantity that might depend on k.

For all three materials, σ^2 decreases with pressure in accordance with the expectation that with increasing pressure the amplitude of atomic oscillations decreases and with it the variance of the nearest-neighbor distance, or "bond length." When the $B1$-$B2$ phase transition sets in (indicated by vertical dotted lines), σ^2 jumps to larger values. This is associated with an increase of the nearest-neighbor distance of a few percent. The next-nearest-neighbor distance, however, decreases considerably so that the overall volume decreases. The other curves in Figs. 6–8 are model calculations of σ^2 from in-

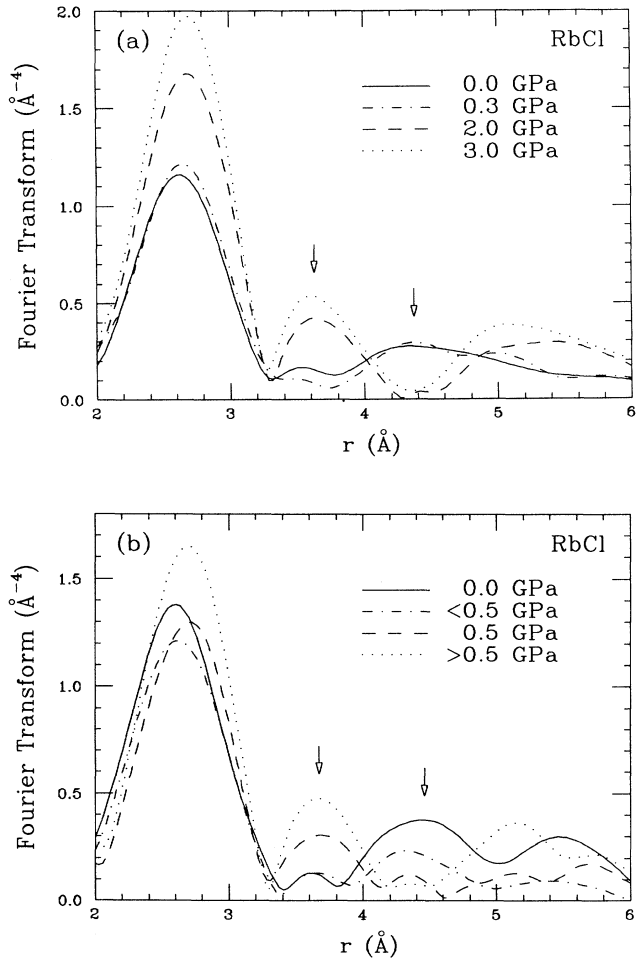

FIG. 4. Magnitudes of the Fourier transform of $\chi(k)k^3$ for RbCl below and above the $B1$-$B2$ structural phase transition at 0.5 GPa. In (a) only pure phases are shown. The dash-dotted and dashed curves in (b) show the RbCl system in the middle of the transition as the second shell moves to a smaller distance and the first shell moves to a large distance. The positions of the second shell are indicated by arrows. The EXAFS phase shift has not been removed.

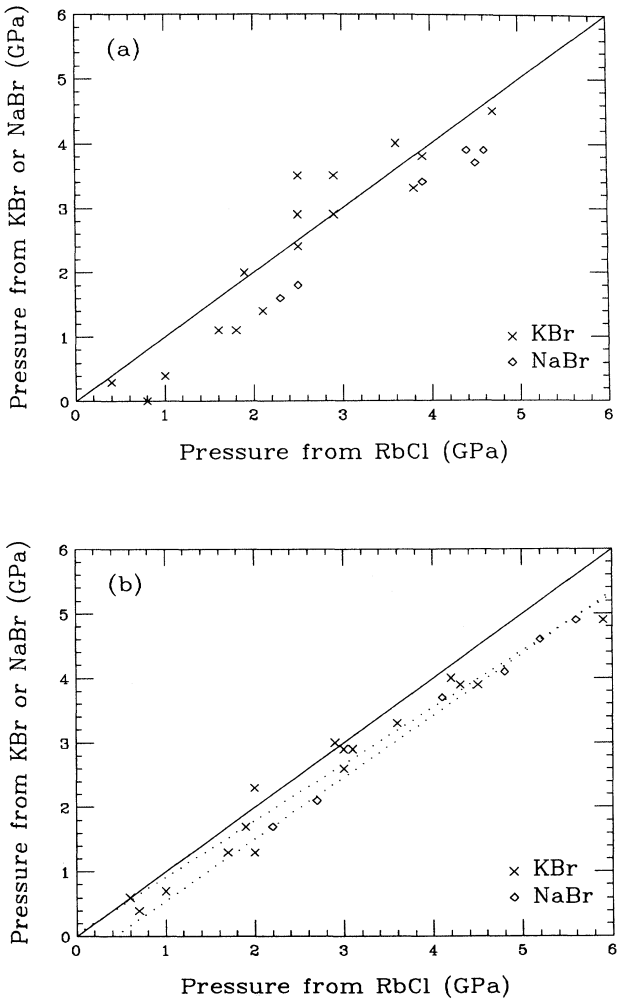

FIG. 5. Pressures determined from samples containing KBr and RbCl (crosses) and NaBr and RbCl (diamonds), respectively. Third cumulants were ignored in (a), included in (b). The dotted lines in (b) are straight-line fits of the KBr+RbCl and NaBr+RbCl data, respectively.

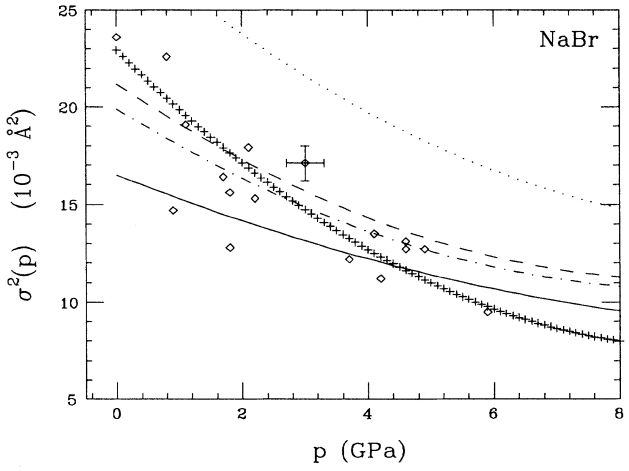

FIG. 6. The second cumulant $\sigma^2(p)$ of NaBr. Comparison of EXAFS measurements (diamonds and crosses) with classical-statistical-mechanics calculations (lines), as described in the text.

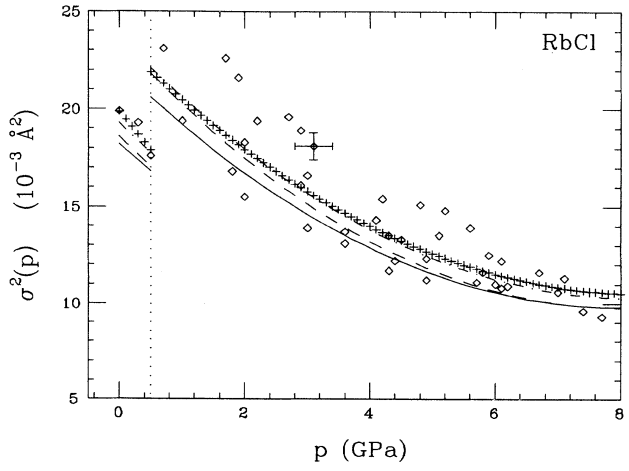

FIG. 8. The second cumulant $\sigma^2(p)$ of RbCl. Comparison of EXAFS measurements (diamonds and crosses) with classical-statistical-mechanics calculations (lines), as described in the text.

teratomic pair and three-body potentials, detailed in the following section.

It is debatable whether the absolute values of the third cumulants $\sigma^{(3)}$ can be extracted from EXAFS. The fit results of $\sigma^{(3)}$ differ quite considerably between experiments, even when the data preparation is the same for all sets. As opposed to σ^2, changes of the Fourier forward transform and backtransform parameters and the fit range change $\sigma^{(3)}$ markedly, namely by about $(1-2)\times 10^{-4}$ Å^{-3}, i.e., by about as much as the absolute value itself. Since zero pressure is the only pressure that was repeated often enough to allow averaging, results for $\sigma^{(3)}(0)$ are the only ones presented in Table I. The error margins include statistical and systematic errors. Also shown in Table I are model calculations of $\sigma^{(3)}$, as explained in the next section.

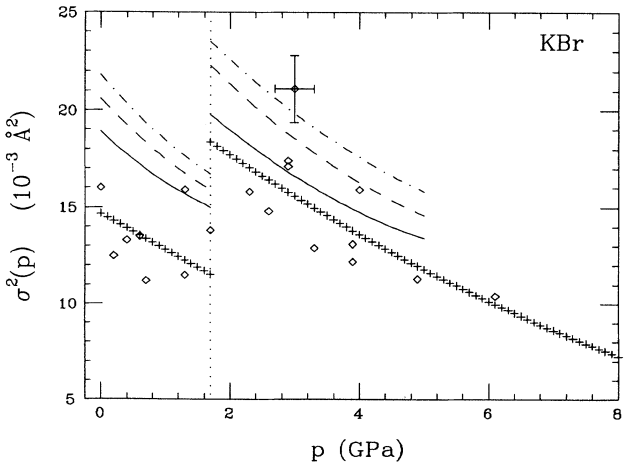

FIG. 7. The second cumulant $\sigma^2(p)$ of KBr. Comparison of EXAFS measurements (diamonds and crosses) with classical-statistical-mechanics calculations (lines), as described in the text.

The nearest-neighbor distances R_1, with and without inclusion of $\sigma^{(3)}$ in the fitting, along with the accurate literature values, are also included in Table I. Statistical and systematic errors are of approximately the same size and are included in the error bars. Note that pressures were not determined from the absolute values of R_1 but from the differences between the absolute values ΔR_1 which can be determined much more accurately. It is obvious that inclusion of $\sigma^{(3)}$ into the fitting procedure results in numbers for R_1 closer to the correct values. It is also interesting to note that the difference between fitted and literature values of R_1 is particularly large for KBr. Since KBr also had the smallest amplitude-correction factor f we suspect that the F_{eff} calculations of the potassium backscatter phase and amplitude have a problem.

We conclude this discussion with the statement that, in fitting cumulants to the experimental data, there must always be concern about their uniqueness. If third and higher cumulants exist, then the magnitudes of the cumulants will depend upon the fitting range. This occurs because the cumulant expansion is an expansion about $k=0$ and will diverge at sufficiently high k values.[32] Caution must be exercised in attributing physical significance to the cumulants. For the alkali halides, tests with various fit ranges indicate that $\sigma^2(p)$ is physically meaningful, but, as indicated above, there is concern for $\sigma^{(3)}$.

IV. MODELING OF CUMULANTS

The absolute values of $\sigma^2(p)$ and $\sigma^{(3)}(0)$ having been extracted as described above, we now want to turn our attention to theoretical attempts to model these quantities. Two methods to calculate the relative changes of the second cumulant have been expounded in our previous

TABLE I. Third cumulants at zero pressure, $\sigma^{(3)}(0)$, from EXAFS and from potential-model calculations, as well as the influence of $\sigma^{(3)}(0)$ on the correct determination of the nearest-neighbor distances. Error margins of experimental and theoretical results include statistical and systematic contributions.

	Third cumulants at zero pressure (10^{-4} Å^3)		
	NaBr	KBr	RbCl
EXAFS experiment	9.6±6	6.0±1	3.9±3
Boswarva	7.0±5	9.0±5	8.7±5
Boswarva + three-body	9.8±5	11.5±5	9.5±5
Tosi and Fumi	11.0±5	10.7±5	9.3±5
Tosi and Fumi + three-body	29.8±7		

	Nearest-neighbor distances at zero pressure (Å)		
	NaBr	KBr	RbCl
Without third cumulant	2.964±0.005	3.218±0.015	3.266±0.005
With third cumulant	2.978±0.005	3.243±0.015	3.275±0.005
Literature value (Ref. 31)	2.987±0.000	3.300±0.000	3.295±0.000

paper.[20] Here we want to go beyond some of the simplifying assumptions underlying these calculations and try to derive the absolute values of the second and third cumulants from first principles.

The second and third cumulants are expressed in terms of the first, second, and third moments (μ_1, μ_2, and μ_3, respectively) by

$$\sigma^2=\mu_2-\mu_1^2 , \tag{2a}$$

$$\sigma^{(3)}=\mu_3-3\mu_2\mu_1+2\mu_1^3 . \tag{2b}$$

The nth moment of the distance between two atoms at positions $\mathbf{r}_1$ and $\mathbf{r}_2$ in a crystal consisting of N atoms is defined as

$$\mu_n(p)=\frac{\int\cdots\int|\mathbf{r}_2-\mathbf{r}_1|^n\exp\{-[p\,\Delta V(\mathbf{r}_1,\ldots,\mathbf{r}_N)+\Delta U(\mathbf{r}_1,\ldots,\mathbf{r}_N)]/k_BT\}\,d\mathbf{r}_1\cdots d\mathbf{r}_N}{\int\cdots\int\exp\{-[p\,\Delta V(\mathbf{r}_1,\ldots,\mathbf{r}_N)+\Delta U(\mathbf{r}_1,\ldots,\mathbf{r}_N)]/k_BT\}\,d\mathbf{r}_1\cdots d\mathbf{r}_N} , \tag{3}$$

where p and V are pressure and volume, respectively, and U is the potential energy of the crystals, which will be discussed in detail later. The integrations are over all $3N$ dimensions of configuration space. The only assumption entering this ansatz is the classical approximation (summation replaced by integration) which is generally justified above the Debye temperature, Θ_D. With Θ_D being 173, 224, and 165 K for KBr, NaBr, and RbCl, respectively,[33] no problems should arise. Note that in our previous paper[20] four rather restrictive assumptions had to be made at this point.

The integral is obviously too complicated to be solved analytically and so a Monte Carlo technique is employed. Monte Carlo integrations of liquid[34–37] and solid[38,39] alkali-metal halides can be found in the literature. In order to facilitate convergence within a finite time, an extra integration variable, volume, is usually introduced in such a way that a tentatively assumed lattice constant is multiplied by a randomly chosen constant factor. Then the integration ranges of the atom positions, $\mathbf{r}_i$ are restricted to the immediate vicinities of their equilibrium positions. In our case, the pressure-volume relation is perfectly well known, and it would be uneconomical to rederive it with this calculation. Therefore, we take the lattice constant as a function of pressure as a fixed input, which eliminates the $p\,\Delta V$ terms from the numerator and denominator in Eq. (2). Then we assign random positions to the atoms in the vicinities of their equilibrium positions.

Three technical problems remain: (i) How large should N be? (ii) Does the integration then have to extend over all $3N$ variables? (iii) How large should the integration range be for each variable $\mathbf{r}_i$? The answer to question (i) depends strongly on the potential energy of the crystal. Therefore we want to discuss the best choice of the potential energy first.

As long as the ions are considered rigid, i.e., undeformable and unpolarizable, the Hamiltonian can be broken down into $N(N-1)/2$ pair potentials. Each pair consists of an electrostatic part, a repulsive part due to core-core overlap, and a van der Waals part. The latter has to do with the fact that both cations and anions have closed electronic shells like noble-gas atoms. When averaged over the entire crystal, the ratios of these three energies

are about (−100):15:(−5). The contribution of ion i to the total electrostatic energy, U_{est}, of the crystal is given by

$$U_{\text{est}}=\frac{1}{2}\sum_{\substack{j=1\\(j\neq i)}}^{N}\frac{e^2}{4\pi\epsilon_0}\frac{1}{r_{ij}}\ , \tag{4}$$

provided the chemical binding is purely ionic.

No exact formulation is available for the core-core repulsion term (also called Born repulsive energy), giving rise to a multitude of empirical formulations and parametrizations. The most often quoted paper is that of Tosi and Fumi[40] presenting the generalized Huggins-Mayer form of the Born repulsive energy. The contribution of a positive or negative ion i to the repulsive energy U_{rep}, of the crystal is given, respectively, by

$$U^{+}_{\text{rep}}=\frac{1}{2}\sum_{j=1}^{N_1}c_{+-}b\exp\left[\frac{r_{+}+r_{-}-r_{ij}}{\rho}\right]+\frac{1}{2}\sum_{k=1}^{N_2}c_{++}b\exp\left[\frac{2r_{+}-r_{ik}}{\rho}\right] \tag{5a}$$

and

$$U^{-}_{\text{rep}}=\frac{1}{2}\sum_{j=1}^{N_1}c_{+-}b\exp\left[\frac{r_{+}+r_{-}-r_{ij}}{\rho}\right]+\frac{1}{2}\sum_{k=1}^{N_2}c_{--}b\exp\left[\frac{2r_{-}-r_{ik}}{\rho}\right], \tag{5b}$$

where N_1 and N_2 are the numbers of nearest and next-nearest neighbors, respectively; c_{++}, c_{+-}, and c_{--}, the Pauling coefficients;[41] b, the repulsive strength parameter; r_+ and r_-, the basic radii; and ρ, the hardness parameter. For clarity, nearest and next-nearest neighbors were indexed with different variables, j and k, respectively.

Several similar such repulsive-energy formulations can be found in the literature;[42–49] we made our choice for the generalized Huggins-Mayer form which is most often used in the literature. Repulsive strength parameters, basic radii, and hardness parameters (and similar such parameters in the other formulations), are generally determined from fitting experimental data. For example, the bulk modulus, its temperature and pressure derivatives, and the volume thermal-expansion coefficient can serve as inputs for the vibrational Hildebrandt equation of state and its volume derivative at constant pressure.[42] Or the dielectric constants, ϵ_0 and ϵ_∞, and the transverse optic frequency, ω_∞, can be used in a different formalism.[45] Many other possibilities exist. Different parametrizations, i.e., parameter values, for a given core-core repulsion term are the result. Parametrizations for the generalized Huggins-Mayer potential, e.g., were reported several times,[40,50,51] the one by Boswarva[50] being considered as particularly reliable for the calculation of the isothermal equation of state[52] and the equation of state.[53] We chose Tosi's[40] and Boswarva's[50] for comparison (see Table II).

Finally, the van der Waals contribution to the potential energy is usually written as a sum of two terms: a dipole-dipole term proportional to the inverse sixth power of the distance, and a dipole-quadrupole term proportional to the inverse eighth power. The contribution of a positive or negative ion i to the van der Waals energy, U_{vdW}, of the crystal is given, respectively, by

$$U^{+}_{\text{vdW}}=\frac{1}{2}\sum_{j=1}^{N_1}\left[\frac{C_{++}}{r_{ij}^6}+\frac{D_{++}}{r_{ij}^8}\right]+\frac{1}{2}\sum_{k=1}^{N_2}\left[\frac{C_{+-}}{r_{ik}^6}+\frac{D_{+-}}{r_{ik}^8}\right] \tag{6a}$$

and

$$U^{-}_{\text{vdW}}=\frac{1}{2}\sum_{j=1}^{N_1}\left[\frac{C_{--}}{r_{ij}^6}+\frac{D_{--}}{r_{ij}^8}\right]+\frac{1}{2}\sum_{k=1}^{N_2}\left[\frac{C_{+-}}{r_{ik}^6}+\frac{D_{+-}}{r_{ik}^8}\right]. \tag{6b}$$

The C's and D's have to be calculated from theory, but, depending on the assumptions underlying the theories, the results differ vastly. We used the values calculated by Boswarva and Murthy[54] but refer to Shanker and Agrawal[55] for a thorough comparison of van der Waals coefficients.

In addition to pair potentials, many-body interactions, in particular, three-body interactions, have been invoked in recent years to improve the accuracy of potential-energy formulations. The most notable example for the necessity of higher-order terms in the Hamiltonian is the so-called Cauchy deviation, $\Delta=C_{12}-C_{44}$, where C_{12} and C_{44} are elastic constants. Δ is invariably zero when many-body interactions are disregarded. Nonzero values are observed experimentally. A comprehensive review of many-body interactions in binary ionic solids is given by Singh,[56] along with heuristic attempts to visualize the physics involved. Our freedom in choosing a three-body formalism was limited by the availability of parametrizations. We found readily available parameters only for the deformation shell model[57–59] and for the charge-transfer model, which dates back to the classic paper of Lundqvist[60] and was applied several times.[61–66] It is difficult to judge to what extent the different many-body formalisms are complementary. We chose to use the charge-transfer model exclusively.

The idea of charge transfer is the following: Consider a cation with Y protons and $Y-1$ electrons and an anion with Z protons and $Z+1$ electrons. As the cation moves toward the anion a transfer of ε electronic charge occurs, the cation being described by $(Y-1-\varepsilon)$ and the anion by $(Z+1+\varepsilon)$ electrons. Since the charges determine the Coulomb interaction, charge transfer gives rise to a correction term to the Coulomb energy, as follows:

$$U_{\text{est}+3b}=\frac{1}{2}\sum_{\substack{j=1\\(j\neq i)}}^{N}\frac{e^2}{4\pi\epsilon_0}\frac{1}{r_{ij}}\left[1+2f_0\sum_{k=1}^{N_1}\exp\left[-\frac{r_{ik}}{\rho}\right]\right]. \tag{7}$$

The summation in the correction term is over the nearest neighbors of atom i. Equation (7) indicates that charge

transfer is not even zero when the ions are in their equilibrium positions. The parameter f_0 can either be calculated from parameter fitting,[61] similar to the pair-potential parameters mentioned above, or from an evaluation of the overlap integral.[62] The results are vastly different, suggesting that parameter fitting is unreliable when it comes to a small correction term like f_0. So we chose the theoretical values.

We can now return to the three open questions about the implementation of the Monte Carlo integration. Since U_{rep}, U_{vdW}, and the term that gives rise to the three-body potential are dependent on nearest- and next-nearest-neighbor interactions only, the number of ions N required to model the crystal potential energy satisfactorily is determined by our ability to get a good representation for the Coulomb energy over as small a crystal volume as possible. Note that a value of the Madelung constant does not solve the problem because the ions are not at their equilibrium positions. While the Ewald method seems to be required for (liquid or solid) alkali-metal halides at high temperatures, the simpler Evjen method[67] is satisfactory for our purpose. It is a double summation in real space and avoids the lack of convergence of such a summation by using fractional charges along the faces of the crystal. The application of this method to the NaCl structure is trivial. In the CsCl structure, two different limits are approached, depending on whether or not the faces consist of ions with the charge of the central particle. The actual limit is then the average of these two limits. When the Evjen method is applied to a grid made up of $5\times5\times5$ ions (NaCl structure) or $5\times5\times5$ bases of 2 ions each (CsCl structure) the electrostatic energy can be calculated with an accuracy of 0.24% and 0.21%, respectively, for the ion at the center in a crystal at rest.

The problem of having to deal with a large number, i.e., $3N$, integration variables cannot completely be overcome with the Monte Carlo technique. If m steps are required to get a reasonable approximation for the integral of a smooth function in one dimension, m^{3N} steps are required in $3N$-dimensional space. Therefore, only a small number of dimensions can be kept variable or, in physical language, only some atoms at the center of the crystal can be allowed to oscillate in a fixed grid of neighbors.

TABLE II. Input for the potential-energy models used: c_{++}, c_{+-}, and c_{--} are the Pauling coefficients; b, the repulsive strength parameter; r_+ and r_-, the basic radii; ρ, the hardness parameter; C_{++}, C_{+-}, and C_{--}, the van der Waals coefficients for the dipole-dipole term; and D_{++}, D_{+-}, and D_{--}, the van der Waals coefficients for the dipole-quadrupole term. f_0 is the three-body potential parameter.

	Pauling (1928)		
	NaBr	KBr	RbCl
c_{++}	1.25	1.25	1.25
c_{+-}	1.00	1.00	1.00
c_{--}	0.75	0.75	0.75

	Tosi and Fumi (1964)			Boswarva (1981)		
	NaBr	KBr	RbCl	NaBr	KBr	RbCl
$b(10^{-19}$ J/bond)	0.338	0.338	0.338	0.203	0.203	0.203
r_+ (Å)	1.170	1.463	1.587	1.339	1.638	1.755
r_- (Å)	1.716	1.716	1.585	1.754	1.754	1.608
ρ (Å)	0.340	0.335	0.318	0.328	0.341	0.327

	Boswarva and Murthy (1981)		
	NaBr	KBr	RbCl
C_{++} (10^{-19} J Å^6/bond)	3.80	36.4	69.9
C_{+-} (10^{-19} J Å^6/bond)	22.2	78.9	85.0
C_{--} (10^{-19} J Å^6/bond)	216.7	253.0	153.8
D_{++} (10^{-19} J Å^8/bond)	3.35	54.4	120.0
D_{+-} (10^{-19} J Å^8/bond)	48.9	197.3	211.3
D_{--} (10^{-19} J Å^8/bond)	715.7	715.7	372.0

	Shanker, Jain, and Singh (1980)		
	NaBr	KBr	RbCl
f_0	11.44	17.82	10.65

Table III shows six model calculations for RbCl with different degrees of freedom. In the two-ion model all spatial coordinates of two neighboring ions at the center of the crystal are kept variable. In the first four-ion model the same is done with 4 ions in a line. The second four-ion model reduces the degrees of freedom from 12 to 8 by freezing the y and z coordinates of the ions at the end of the line (with the ions being aligned along the x axis), and so on. All six models were calculated with the same sequence of random configurations. Therefore the differences between the results are free from randomness and represent exclusively the differences between the models. The potential parameters of Boswarva[50] were used without a three-body term.

Table III presents the second cumulants of the nearest-neighbor distance σ^2 at 0 and 8 GPa, along with error bars representing random errors. It seems that σ^2 depends somewhat on the number of ions, but for 6 and more ions the systematic error decreases sufficiently and is not more than $(0.5-1.0)\times10^{-3}$ Å^2. Together with a random error of the same size, the six-ion model in 10 dimensions produces a total error of about 1.5×10^{-3} Å^2 and was chosen for our calculations. Similarly, the total error for $\sigma^{(3)}$ was determined to be about 5×10^{-4} Å^3 and entered in Table I. The final choice for the crystal sizes was therefore $10\times5\times5$ for the NaCl structure and $7\times7\times7$ ($\times2$ ions each in the bases) for the CsCl structure, with the ions being lined up along the x axis in the former and along the diagonal in the latter.

Finally, the best choice of integration range for the integrals in Eq. (3) must be discussed. Figure 9 shows the result for σ^2 of RbCl at $p=0$, with each diamond symbol representing the average of 5000 random configurations. σ^2 first increases with increasing integration range, indicating that it is still too small and configurations with non-negligible statistical weights (Boltzmann factors) have been omitted. After a certain critical value (designated by a dotted line), σ^2 remains constant, but its variance is increasing as more and more configurations with small weights are sampled. The correct result for σ^2 is then obtained by averaging over all results above the dotted line (i.e., a total of 140 000 configurations) taking the appropriate Boltzmann factors as weights. This average is shown by the dashed line.

V. MODELING RESULTS AND DISCUSSION

Figures 6–8 and Table I show the results of the cumulant modeling. Calculations of $\sigma^2(p)$ were made for a few points along the pressure axis and joined with polynomials, as shown in the figures. The solid lines show the results for the generalized Huggins-Mayer potential with the parametrization of Boswarva.[50] When the three-body potential of Singh[56] is added, the dash-dotted lines are obtained. Use of Tosi's[40] parametrization of the generalized Huggins-Mayer potential gives the dashed lines as result. Finally, the dotted lines are obtained by combining Tosi's parameters and Singh's three-body term. The sequence of random configurations was repeated identically for all pressures and all curves. This eliminates *random* errors between the curves and minimizes *random* errors between the pressures.

TABLE III. Monte Carlo results of the second cumulants of the nearest-neighbor distances, σ^2 at 0 and 8 GPa. Calculations were made for RbCl with the Boswarva parameters of the pair potential. No three-body potential was applied. The models differ by the number of ions that are allowed to move freely in the directions specified.

Model	Coordinate	Degrees of freedom	σ^2(0 GPa) (10^{-3} Å^2)	σ^2(8 GPa) (10^{-3} Å^2)
2 ions	x	++	20.1±0.3	10.1±0.4
	y	++		
	z	++		
4 ions	x	++++	22.1±0.5	9.0±0.6
	y	++++		
	z	++++		
4 ions	x	++++	21.6±0.6	10.4±0.7
	y	++		
	z	++		
6 ions	x	++++++	19.1±0.4	9.5±1.1
	y	++		
	z	++		
6 ions	x	++++++	18.6±0.7	
	y	++++		
	z	++++		
8 ions	x	+++++++	20.1±1.6	
	y	++		
	z	++		

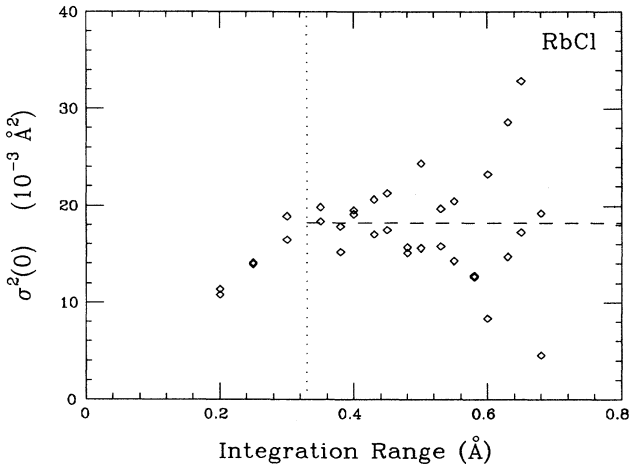

FIG. 9. Calculation of σ^2 at $p=0$ for RbCl with the pair-potential parameters of Boswarva and without a three-body potential. Each point represents the weighted average of 5000 configurations. The ions are free to assume any position inside the integration range, as specified. For too small integration ranges, statistically significant configurations are omitted, thus producing too small values for σ^2. For integration ranges above the dotted line, more and more statistically insignificant configurations increase the spread of the points. The final result for σ^2 is then the weighted average of all points above the dotted line, as indicated by the dashed line.

Let us now compare experimental and model results. An inspection of Fig. 6 (NaBr) shows that the four curves are further apart than the total error in the modeled σ^2 (1.5×10^{-3} Å^2) would allow. This indicates that the model calculations are sensitive to the potential models and parameters used. The experimental data match the modeled ones only moderately well with the absolute values of σ^2 being similar but the slope being markedly larger. A different formulation of the pair potential and/or the three-body potential may be required to obtain a larger slope and improve the match with the experiment.

For KBr (Fig. 7), differences between the two pair-potential-parameter calculations and the three-body calculation are a little bit smaller than in NaBr. Experiment and one model calculation match closely in the $B2$ phase. However, a systematic offset exists between the experiment and the model calculations in the $B1$ phase. Since the slopes of experimental data and model results are fairly similar, it may well be that the existing potential formulation along with different parameters can fit the experimental results in both phases.

Finally, a reasonable match of experiment and model calculations exists for σ^2 of RbCl (Fig. 8). This may be due in part to the fact that we made more experiments with RbCl than with NaBr and KBr. But, interestingly enough, there is also little disagreement between the model calculations themselves.

Experimental and modeled values of $\sigma^{(3)}(0)$ agree well for NaBr, with the exception of the Tosi-Fumi pair potential combined with the three-body potential. This combination gave already unacceptable results for $\sigma^{(2)}(p)$. For KBr and RbCl, experimental and model results differ by about a factor of 2. Since the absolute values of $\sigma^2(p)$ are not too different between the three materials investigated, we expect the same to be true for $\sigma^{(3)}(0)$ and therefore tend to dismiss the low EXAFS results.

We observe that high-pressure EXAFS, due to its sensitivity to interatomic potentials, can permit assessment of existing interatomic-potential-parameter formulations and parametrizations. Many attempts have been made to evaluate and fit potential parameters from a knowledge of the cohesive energy. But the cohesive energy does not depend strongly on potential parameters. The sensitivity on potential parameters increases with the order of the spatial derivative of the potential energy: Second-order elastic constants (second derivative; SOEC), third-order elastic constants (TOEC) and first derivatives of SOEC (third derivative), and finally fourth-order elastic constants along with first derivatives of TOEC and second derivatives of SOEC (fourth derivative) are successively more sensitive to the forces between atoms. That is why elastic constants and their derivatives have been calculated repeatedly from alkali-metal halide potentials[46,51,59,61–63,66,68–70] and compared with results from ultrasound measurements. Also, dielectric constants and their derivatives,[52,66] phase-transition pressures,[58,59,64,65] and other parameters have been found useful. All the above-mentioned calculations share one common characteristic: Physical quantities are calculated for *one* thermodynamic condition, mostly STP. In other words, no continuous functions of pressure or temperature are calculated.

The only continuous function of pressure that is calculated from potential parameters is the pressure-volume relation (isothermal equations of state).[43,49,52,53,71] Since volume depends only on the first moment (which is identical to the first cumulant) of the nearest-neighbor distance, we can also call a pressure-volume relation the pressure dependence of the first cumulant. Following the logic of our previous paper,[20] the second cumulant is proportional to the first pressure derivative of the first cumulant [Eq. (19)]. Calling to mind that this relation is based on rather restrictive assumptions, we want to use it only *qualitatively* to show that the second EXAFS cumulant is more sensitive to potential parameters than the pressure-volume relation.

Eggenhoffner *et al.*'s[72,73] comparative study and evaluation of various pair-potential models concludes with the words, ". . . it is clearly difficult to say which, if any, of the new potentials . . . is to be preferred over the others. It is also difficult to say whether the new potentials taken as a whole have truly improved our knowledge of the effective short-range pair interaction potentials in the alkali-metal halides." While we have no indication that our knowledge of alkali-metal halide potentials has improved in the decade since this remark, we can now offer an additional sensitive physical parameter, $\sigma^2(p)$, to assess existing pair potentials and, possibly in the future, to calculate better ones.

ACKNOWLEDGMENTS

We would like to thank N. Alberding, A. J. Seary, K. R. Bauchspiess, and D. Jiang, our collaborators from Simon Fraser University, and J. E. Whitmore, J. M. Tranquada, and B. Houser, our University of Washington group, for having done the experiments with us at SSRL and J. M. Tranquada for having started with the data analysis.[74] We also like to thank J. J. Rehr for valuable discussions. This work was supported by Department of Energy Grants No. DE-AT06-83ER45038 and No. DE-FG06-84ER45163, and by the Natural Science and Engineering Research Council of Canada. SSRL is supported by the U.S. Department of Energy (Office of Basic Energy Sciences) and the National Institutes of Health (Biotechnology Research Program, Division of Research Resources).

*Present address: Fachbereich Physik, Universität Paderborn, W-4790 Paderborn, Germany.

[1]J. P. Itié, M. Jean-Louis, E. Dartyge, A. Fontaine, and A. Jucha, J. Phys. (Paris) Colloq. Suppl. 12 **47**, C8-897 (1986).

[2]F. Baudelet *et al.*, Z. Phys. B **69**, 141 (1987).

[3]J. P. Itié, A. Polian, G. Calas, J. Petiau, A. Fontaine, and H. Tolentino, Phys. Rev. Lett. **63**, 398 (1989).

[4]J. P. Itié, A. Polian, C. Jauberthie-Carillon, E. Dartyge, A. Fontaine, H. Tolentino, and G. Tourillon, Physica B **158**, 604 (1989).

[5]J. P. Itié, A. Polian, C. Jauberthie-Carillon, E. Dartyge, A. Fontaine, H. Tolentino, and G. Tourillon, Phys. Rev. B **40**, 9709 (1989).

[6]A. Polian, J. P. Itié, E. Dartyge, A. Fontaine, and G. Tourillon, Physica B **158**, 525 (1989).

[7]A. Polian, J. P. Itié, E. Dartyge, A. Fontaine, and G. Tourillon, Phys. Rev. B **39**, 3369 (1989).

[8]A. Polian, J. P. Itié, C. Jauberthie-Carillon, E. Dartyge, A. Fontaine, and H. Tolentino, High Press. Res. **4**, 309 (1990).

[9]J. P. Itié, A. Polian, G. Calas, J. Petiau, A. Fontaine, and H. Tolentino, High Press. Res. **5**, 717 (1990).

[10]S. Sueno, I. Nakai, M. Imafuku, H. Morikawa, M. Kimata, K. Ohsumi, M. Nomura, and O. Shimomura, Chem. Lett. **10**, 1663 (1986).

[11]K. Ohsumi, S. Sueno, I. Nakai, M. Imafuku, H. Morikawa, M. Kimata, M. Nomura, and O. Shimomura, J. Phys. (Paris) Colloq. Suppl. 12 **47**, C8-189 (1986).

[12]N. Alberding, E. D. Crozier, R. Ingalls, and B. Houser, J. Phys. (Paris) Colloq. Suppl. 12 **47**, C8-681 (1986).

[13]K. R. Bauchspiess, E. D. Crozier, and R. Ingalls, J. Phys. (Paris) Colloq. Suppl. 12 **47**, C8-975 (1986).

[14]R. Ingalls, E. D. Crozier, and A. J. Seary, Physica B **139&140**, 505 (1986).

[15]J. M. Tranquada and R. Ingalls, Phys. Rev. B **34**, 4267 (1986).

[16]B. Houser, N. Alberding, R. Ingalls, and E. D. Crozier, Phys. Rev. B **37**, 6513 (1988).

[17]R. Ingalls, E. D. Crozier, N. Alberding, A. J. Seary, K. R. Bauchspiess, B. Houser, and J. Freund, *High Pressure Science and Technology: Proceedings of the XIth AIRAPT International Conference* (Naukova Dumka, Kiev, 1989), Vol. 2, p. 327.

[18]N. Alberding *et al.*, Physica B **158**, 463 (1989).

[19]K. R. Bauchspiess, E. D. Crozier, and R. Ingalls, Physica B **158**, 492 (1989).

[20]J. Freund, R. Ingalls, and E. D. Crozier, Phys. Rev. B **39**, 12 537 (1989).

[21]J. Freund, R. Ingalls, and E. D. Crozier, J. Phys. Chem. **94**, 1087 (1990).

[22]J. Freund and R. Ingalls, High Press. Res. **5**, 785 (1990).

[23]R. Ingalls, E. D. Crozier, J. E. Whitmore, A. J. Seary, and J. M. Tranquada, J. Appl. Phys. **51**, 3158 (1980).

[24]IMSL, Inc., 2500 Park West Tower One, 2500 City West Boulevard, Houston, Texas 77042-3020.

[25]J. W. Cook, Jr. and D. E. Sayers, J. Appl. Phys. **52**, 5024 (1981).

[26]W. H. McMaster, N. Kerr DelGrande, J. H. Mallett, and J. H. Hubbell, Compilation of X-Ray Cross Sections, Lawrence Livermore Laboratory, 1969.

[27]J. J. Rehr, R. C. Albers, and J. Mustre de Leon, Physica B **158**, 417 (1989).

[28]F. D. Murnaghan, Proc. Natl. Acad. Sci. U.S.A. **30**, 244 (1944).

[29]S. N. Vaidya and G. C. Kennedy, J. Phys. Chem. Solids **32**, 951 (1971).

[30]C. W. F. T. Pistorius, Prog. Solid State Chem. **11**, 1 (1976).

[31]L. Merrill, J. Phys. Chem. Ref. Data **6**, 1205 (1977).

[32]E. D. Crozier, J. J. Rehr, and R. Ingalls, in *X-Ray Absorption*, edited by D. C. Koningsberger and R. Prins (Wiley, New York, 1988), p. 373.

[33]N. W. Ashcroft and N. D. Mermin, *Solid State Physics* (Holt, Rinehart and Winston, New York, 1976), p. 459.

[34]W. W. Wood, in *Physics of Simple Liquids*, edited by H. N. V. Temperley, J. S. Rowlinson, and G. S. Rushbrooke (Wiley, New York, and North-Holland, Amsterdam, 1968), p. 115.

[35]L. V. Woodcock and K. Singer, Trans. Faraday Soc. **67**, 12 (1971).

[36]B. Hafskjold and G. Stell, in *The Liquid State of Matter*, edited by E. W. Montroll and J. L. Lebowitz (North-Holland, Amsterdam, 1982), p. 175.

[37]A. Baranyai, I. Ruff, and R. L. McGreevy, J. Phys. C **19**, 453 (1986).

[38]D. J. Adams and I. R. McDonald, J. Phys. C **7**, 2761 (1974).

[39]S. Yashonath and C. N. R. Rao, Mol. Phys. **54**, 245 (1985).

[40]M. P. Tosi and F. G. Fumi, J. Phys. Chem. Solids **25**, 45 (1964).

[41]L. Pauling, Proc. Am. Chem. Soc. **50**, 1036 (1928).

[42]F. G. Fumi and M. P. Tosi, J. Phys. Chem. Solids **25**, 31 (1964).

[43]D. L. Decker, J. Appl. Phys. **36**, 157 (1965).

[44]C. R. A. Catlow, K. M. Diller, and M. J. Norgett, J. Phys. C **10**, 1395 (1977).

[45]M. J. L. Sangster, U. Schröder, and R. M. Atwood, J. Phys. C **11**, 1523 (1978).

[46]M. J. L. Sangster and R. M. Atwood, J. Phys. C **11**, 1541 (1978).

[47]Y. V. G. S. Murti and T. V. Selvarajan, Phys. Status Solidi B **108**, 315 (1981).

[48]J. Shanker and K. Singh, J. Inorg. Nucl. Chem. **43**, 1445 (1981).

[49]J. Shanker, J. Narain, and A. K. Rajauria, Phys. Status Solidi B **122**, 435 (1984).

[50]I. M. Boswarva, J. Phys. Chem. Solids **42**, 487 (1981).

[51]R. K. Gupta, A. Shiromany, P. S. Bakhshi, and J. Shanker, Phys. Status Solidi B **127**, 473 (1985).

[52]A. Shiromany, G. M. S. Srivastava, and J. Shanker, Phys. Status Solidi B **135**, 119 (1986).
[53]M. Kumar, A. K. Pachauri, S. D. Chaturvedi, and A. K. Sharma, Phys. Status Solidi B **146**, 125 (1988).
[54]I. M. Boswarva and C. S. N. Murthy, J. Phys. Chem. Solids **42**, 109 (1981).
[55]J. Shanker and G. G. Agrawal, Phys. Status Solidi B **123**, 11 (1984).
[56]R. K. Singh, Phys. Rep. **85**, 259 (1982).
[57]A. K. Sarkar and S. Sengupta, Solid State Commun. **7**, 135 (1969).
[58]A. K. Sarkar and S. Sengupta, Phys. Status Solidi **36**, 359 (1969).
[59]A. K. Sarkar and S. Sengupta, Phys. Status Solidi B **58**, 775 (1973).
[60]S. O. Lundqvist, Ark. Fys. **12**, 263 (1957).
[61]R. P. Singh and J. Shanker, Phys. Status Solidi B **93**, 373 (1979).
[62]J. Shanker, V. C. Jain, and J. P. Singh, Phys. Rev. B **22**, 1083 (1980).
[63]N. V. K. Prabhakar and R. K. Singh, Phys. Status Solidi B **127**, 95 (1985).
[64]M. Kumar, D. Hans, A. K. Sharma, and J. Shanker, Phys. Status Solidi B **144**, 543 (1987).
[65]G. B. Varshney and J. P. S. Rana, Curr. Sci. **56**, 133 (1987).
[66]D. Hans, A. A. S. Sangachin, and M. Kumar, Phys. Status Solidi B **147**, 529 (1988).
[67]M. P. Tosi, Solid State Phys. **16**, 1 (1964).
[68]J. Shanker, J. P. Singh, and V. P. Gupta, Phys. Status Solidi B **103**, 573 (1981).
[69]A. Cox and M. J. L. Sangster, J. Phys. C **15**, 4473 (1982).
[70]B. R. K. Gupta, Solid State Commun. **54**, 817 (1985).
[71]J. Shanker and K. Singh, Phys. Status Solidi B **115**, 381 (1983).
[72]R. Eggenhoffner, C. S. N. Murthy, and F. G. Fumi, J. Phys. Chem. Solids **39**, 1295 (1978).
[73]R. Eggenhoffner, F. G. Fumi, and C. S. N. Murthy, J. Phys. Chem. Solids **43**, 583 (1982).
[74]J. M. Tranquada, Ph.D. thesis, University of Washington, 1984.